Published in final edited form as:
*Magn Reson Med*. 2014 September ; 72(3): 629–639. doi:10.1002/mrm.24963.

# Localized Spatio-Temporal Constraints for Accelerated CMR Perfusion

**Mehmet Akçakaya**, **Tamer A. Basha**, **Silvio Pflugi**, **Murilo Foppa**, **Kraig V. Kissinger**, **Thomas H. Hauser**, and **Reza Nezafat**
Department of Medicine (Cardiovascular Division), Beth Israel Deaconess Medical Center and Harvard Medical School, Boston, MA

## Abstract

**Purpose—**To develop and evaluate an image reconstruction technique for cardiac MRI (CMR)perfusion that utilizes localized spatio-temporal constraints.

**Methods—**CMR perfusion plays an important role in detecting myocardial ischemia in patients with coronary artery disease. Breath-hold k-t based image acceleration techniques are typically used in CMR perfusion for superior spatial/temporal resolution, and improved coverage. In this study, we propose a novel compressed sensing based image reconstruction technique for CMR perfusion, with applicability to free-breathing examinations. This technique uses local spatio-temporal constraints by regularizing image patches across a small number of dynamics. The technique is compared to conventional dynamic-by-dynamic reconstruction, and sparsity regularization using a temporal principal-component (pc) basis, as well as zerofilled data in multi-slice 2D and 3D CMR perfusion. Qualitative image scores are used (1=poor, 4=excellent) to evaluate the technique in 3D perfusion in 10 patients and 5 healthy subjects. On 4 healthy subjects, the proposed technique was also compared to a breath-hold multi-slice 2D acquisition with parallel imaging in terms of signal intensity curves.

**Results—**The proposed technique results in images that are superior in terms of spatial and temporal blurring compared to the other techniques, even in free-breathing datasets. The image scores indicate a significant improvement compared to other techniques in 3D perfusion (2.8±0.5 vs. 2.3±0.5 for x-pc regularization, 1.7±0.5 for dynamic-by-dynamic, 1.1±0.2 for zerofilled). Signal intensity curves indicate similar dynamics of uptake between the proposed method with a 3D acquisition and the breath-hold multi-slice 2D acquisition with parallel imaging.

**Conclusion—**The proposed reconstruction utilizes sparsity regularization based on localized information in both spatial and temporal domains for highly-accelerated CMR perfusion with potential utility in free-breathing 3D acquisitions.

### Keywords

cardiac perfusion; free-breathing; compressed sensing

Correspondence to: Reza Nezafat, Ph. D., Beth Israel Deaconess Medical Center, 330 Brookline Ave, Boston, MA, 02215, Phone: 617-667-1747; Fax: 617-975-5480, rnezafat@bidmc.harvard.edu.

## Introduction

Cardiac MRI (CMR) perfusion enables detection of myocardial ischemia in patients with suspected coronary artery disease (CAD) by providing assessment of regional myocardial blood flow (1–3). Clinically, 2D multi-slice saturation-prepared imaging is often used for evaluation of left ventricular (LV) perfusion with 2–4 short-axis slices acquired every R-R interval (4). Parallel imaging techniques (5–7) have been used to improve the coverage, spatial resolution and/or temporal resolution in these acquisitions.

To improve the spatio-temporal resolution and coverage further, k-t based acceleration techniques, such as k-t sensitivity encoding (SENSE) (8) and k-t principal component analysis (PCA) (9), which utilize correlations across the temporal dimension have been applied to perfusion CMR. These techniques utilize a uniform undersampling of the k-space, which varies across different dynamics, resulting in a point-spread-function with lattice structure that leads to a periodic replication of the underlying image (8). The reconstruction then unfolds the resulting overlap of the image in the *x-f* domain (Fourier transform of images along the time direction) using adaptive temporal filtering, with signal correlation information derived from low-resolution training data, as well as multi-coil information (9). For perfusion imaging, the central part of k-space is fully-sampled in each dynamic to generate the training data. These techniques were used to acquire multi-slice 2D images with 5-fold acceleration and $1.4 \times 1.4$ mm$^2$ in-plane resolution, with four slices acquired over two R-R intervals (10). Compressed sensing (CS), which utilizes the compressibility of images in a transform domain for reconstruction from incoherently undersampled data (achieved by random undersampling for Cartesian acquisition) has also been applied to perfusion CMR (11). Using a $B_1$-weighted approach utilizing multi-coil information and sparsity in the *x-f* domain, up to 8-fold acceleration was achieved for the acquisition of 10 slices covering the LV (11). Other advanced reconstruction techniques based on a combination of low-rank regularization and total variation (TV) norm regularization (12), as well as group sparsity (13) have also been used in this context.

While the aforementioned k-t based techniques can be used for high acceleration rates, the use of temporal correlations require that the subsequent dynamics be spatially aligned. This necessitates a prolonged breath-hold acquisition, which may be difficult for many patients. Translational respiratory motion-correction based on an initial reconstruction, generated by *x-f* space regularization, has been proposed as a way of facilitating free-breathing 2D perfusion acquisitions (14). However, the reliance on an initial estimate generated by *x-f* space regularization may reduce the applicability of this technique to highly-accelerated acquisitions, especially in patients with irregular breathing patterns. Rank-based regularization has also been used in acquisitions with breath-holding at the time of injection and free-breathing in later dynamics (12).

Larger coverage of the LV is necessary to fully evaluate the extent of ischemia, which is a strong predictor of outcome (15). 3D CMR perfusion has been proposed for its superior contiguous coverage and higher SNR to potentially improve the estimation of the extent of hypo-perfused tissue (16,17). The contiguous coverage reduces slice misregistration errors compared to 2D imaging, facilitating accurate quantification. However, for adequate spatio-

temporal resolution in 3D perfusion CMR, accelerated imaging is required. Due to the enhanced SNR, parallel imaging techniques that are commonly used for 2D multi-slice imaging can be applied with higher acceleration factors. In (16), a six-fold acceleration factor was used with adaptive sensitivity encoding (6,18), where time-varying coil sensitivity maps are generated using sliding-window reconstructions, to achieve a spatial resolution of 2.3×3.6×10 $mm^3$ with a 312 ms acquisition window on a 1.5T scanner. In (17), an acceleration factor of six was used with 2D sensitivity encoding (19) and adaptive sensitivity encoding (18), to achieve a spatial resolution of 3.0×4.3×10 $mm^3$ in a 304 ms acquisition window at 3T. However, it was noted that such resolution may be insufficient for visualizing sub-endocardial defects.

To further improve the spatio-temporal resolution, k-t based acceleration techniques have been applied to 3D perfusion. In (20), an improved k-t principal PCA reconstruction technique enabled 3D perfusion acquisitions with spatial resolution 2.3×2.3×10 $mm^3$ in a 225 ms acquisition window at 3T. The improved reconstruction accuracy was due to the use of a compartment-based approach, where different spatio-temporal basis functions were derived for distinct spatial compartments of the heart. A combination of k-t SENSE (8) reconstruction and dual-density stack-of-spirals acquisition was used to achieve 2.4×2.4×9 $mm^3$ spatial resolution and 230 ms temporal resolution (21) at 1.5T. $B_1$-weighted CS with *x-f* domain sparsity has also been reported in a feasibility study for 3D perfusion CMR (22). All these k-t based approaches for 3D perfusion CMR have been implemented for breath-hold acquisitions.

In this study, we sought to develop and evaluate a novel CS-based image reconstruction technique for accelerated perfusion CMR with randomly undersampled acquisitions, with applicability to free-breathing examinations. Our reconstruction relies on recent ideas from accelerated MRI reconstruction, which demonstrate that utilizing localized image features, such as compartments across temporal dynamics (20) or image patches across different parts of the volume (23) improve reconstruction quality. We hypothesize that 2D image patches in the imaging volume are slowly-varying across a small number of consecutive heartbeats, even for free-breathing acquisitions, instead of the whole volume being slowly varying across all dynamics as in traditional k-t techniques. We utilize these local spatio-temporal correlations to generate distinct sparsifying bases for different parts of the image volume. This sparsity is then used to regularize a $B_1$-weighted least squares problem. The performance of the proposed technique was first established with free-breathing multi-slice 2D acquisitions. Subsequently, the technique was evaluated in a number of patients, both with breath-held and free-breathing 3D acquisitions.

## Methods

### Proposed Reconstruction Technique

Randomly-undersampled data with incoherent aliasing artifacts can be reconstructed utilizing CS techniques. CS reconstruction solves a regularized least-squares problem, enforcing data consistency with the measured k-space locations, also allowing for the incorporation of coil sensitivities in a $B_1$-weighted approach, and utilizing a sparsifying transform for exploiting the compressibility of the image volume. For perfusion,

conventional CS algorithms use the *x-f* space or the *x-pc* space for sparsification, where the principal components (pc) are derived for the whole volume.

The proposed reconstruction approach utilizes distinct spatio-temporal sparsifying functions based on PCA for different parts of the imaging volume to compensate for various physiological changes. The use of distinct principal component basis for different parts of the imaging volume is depicted in Figure 1. In perfusion imaging, different anatomies exhibit different contrast uptake, resulting in distinct temporal correlations. In compartment-based k-t PCA, this was exploited by defining compartments of interest for RV, LV, myocardium, and others. In the proposed algorithm we extend the use of compartments to $N_b \times N_b$ 2D image patches. This allows us to consider overlapping image patches within the same slice, leading to an overcomplete representation, which was shown to improve reconstruction quality in CS (23). It further facilitates the use of this technique with free-breathing data, since the correct determination of individual compartments for distinct structures such as right ventricle (RV), LV or myocardium as in (20) requires the alignment of different dynamics. The second component of the proposed approach is that only $N_{dyn}$ consequent dynamics are considered when generating the sparsifying transforms, instead of all of the dynamics, as in traditional k-t methods. This is based on the hypothesis that even with moderate free-breathing, the displacement over a small number of consecutive heartbeats will be regular and not severe. Consequent dynamics is used in an overlapping fashion to lead to an overcomplete representation.

The algorithm was implemented in two stages using a boot-strap method (24), where an initial reconstruction is used to generate the distinct principal components for each $N_b \times N_b \times 1 \times N_{dyn}$ overlapping image volumes, as in Figure 1. These bases are subsequently used to sparsify the overlapping image volumes for regularization in the second and final stage of the reconstruction.

**Implementation Details—**Both stages of reconstruction relies on a $B_1$-weighted approach, where the coil sensitivity information is used for data consistency during the reconstruction (11,25). Based on iterative soft thresholding (26), every iteration of the $B_1$-weighted algorithm can be summarized as: 1) The current combined-coil image estimate is de-noised using the regularization function (e.g. TV norm), 2) The combined image is mapped to individual coils via voxel-wise multiplication with the sensitivity map of that coil, 3) Data consistency with the measured data is enforced by Fourier transforming the coil images, replacing the acquired k-space locations with the acquired lines, and inverse Fourier transforming to get data-consistent images, 4) The data-consistent coil images are combined using the coil sensitivity maps, where the voxel-wise product of the coil images and conjugate of the coil sensitivity maps were summed across the coil dimension, to generate the next image estimate. Normalized relative coil sensitivity maps were generated for each dynamic by: Hanning filtering the fully-sampled central k-space of each dynamic in the $k_y$-$k_z$ direction; inverse Fourier transforming these filtered k-space data to get a low-resolution image for each coil; normalizing each coil image by the root-sum-squares combination of all coil images.

For the first stage of the algorithm, a basic estimate of the images was generated, which was then used to derive distinct pc bases for each $N_b \times N_b \times 1 \times N_{dyn}$ overlapping image volumes. For the proposed implementation, $N_b$ was chosen to be 10, and $N_{dyn}$ was set to 5. Two types of basic estimates were compared visually in a pilot study: 1) A CS reconstruction with spatial TV regularization (with TV norm weight = $10^{-4}$ times the maximum absolute voxel intensity value of the zero-filled data) for reconstructing each dynamic individually, 2) A low-resolution image generated from the fully-sampled central k-space lines. Subsequently, the preferred way of generating the basic estimate was used for all the proposed reconstructions.

In the second stage, these distinct pc bases were used for regularization in the $B_1$-weighted algorithm (with the regularization term weight = $10^{-3}$ times the maximum absolute voxel intensity value of the zero-filled data), as described previously. Hence, the first stage of each iteration of the $B_1$-weighted algorithm was modified as follows: Each $N_b \times N_b \times 1 \times N_{dyn}$ overlapping image volume of the current combined-coil image estimate was sparsified using the corresponding pc basis for that volume, thresholded using soft-thresholding, and inverse transformed. These overlapping thresholded volumes were combined by simple averaging to generate the thresholded estimate. The proposed reconstruction was implemented in Matlab (v7.6, MathWorks, Natick, MA).

## In-vivo Imaging

All imaging was performed on a 1.5-T Philips Achieva (Philips Healthcare, Best, The Netherlands) system with a 32-channel cardiac phased-array receiver coil and without vasodilator stress. For this HIPAA-compliant study, the imaging protocol was approved by our institutional review board. Written informed consent was obtained from all participants.

**Accelerated 2D Perfusion—**2D multi-slice perfusion images were acquired on a healthy 21 year-old female subject without contraindications to MRI. After the first few heartbeats, 0.05 mmol/kg gadobenate dimeglumine (MultiHance, Bracco, Rome, Italy) was intravenously injected with a power injector at a rate of 4 mL/s, followed by a 10 mL saline flush. An electrocardiogram (ECG) triggered saturation-recovery gradient-echo (GRE) perfusion sequence was used for acquisition on the LV short axis with anterior-posterior phase encoding. The imaging parameters were: repetition time/echo time/flip angle = 3.2ms/1.6ms/20°, spatial resolution = 1.6×1.6 $mm^2$, slice thickness = 10 mm, number of slices = 5, field-of-view = 320×320 $mm^2$, saturation pre-pulse delay = 100 ms. The acquisition was prospectively accelerated by a rate of 4, by keeping the central 22 k-space lines and randomly undersampling the outer k-space, resulting in an acquisition window of 155 ms per 2D slice. The acquisition was performed with free-breathing and no breath-holding instructions.

**Accelerated 3D Perfusion—**Ten patients (46.7±14.1 years; 7 men) referred for clinical CMR and five healthy subjects (41.6 ± 26.4 years, 2 men) without contraindications to MRI were recruited for 3D rest perfusion CMR. An ECG-triggered saturation-recovery GRE perfusion sequence was used for acquisition. After the first few heartbeats, 0.05 mmol/kg gadobenate dimeglumine (MultiHance, Bracco, Rome, Italy) was intravenously injected

with a power injector at a rate of 4 mL/s, followed by a 10 mL saline flush. A truncated RF excitation pulse (flip angle = 20°) was utilized for a reduced repetition time and echo time of 2.1 ms and 1.2 ms respectively. Images were acquired in the LV short axis with foot-head phase encoding, spatial resolution = 2.3×2.3×10.0 $mm^3$, field of view = 340×340×80 $mm^3$, where the two edge slices were discarded to generate six sectional slices. A saturation prepulse delay of 100 ms was used with an acquisition time of 250 ms per heart beat. Six of the acquisitions were acquired during a breath-hold at the time of injection, whereas the remainder were acquired with free-breathing throughout the scan. The acquisition was performed for 30 seconds, which corresponded to an average number of dynamics of 38 ± 11 (range: 17 and 57). Data acquisition was prospectively accelerated by a rate of 7.5 with respect to an elliptical window (10-fold with respect to the whole k-space) in $k_y$-$k_z$ using a pseudo-randomly generated undersampling pattern. Central k-space of size 11×3 in $k_y$-$k_z$, corresponding to 3.5% of the k-space was fully-sampled, and the outer k-space was randomly undersampled. A modified radial $k_y$-$k_z$ phase reordering scheme, allowing the centermost k-space line to be sampled first, was used to mitigate flow artifacts and Eddy currents by reducing gradient switching (27). Additionally, breath-hold multi-slice 2D perfusion was acquired on four healthy subjects (46.5 ± 27.8 years, 2 men), using the same sequence parameters as the aforementioned 2D sequence, but with SENSE rate 2.7 for accelerated imaging. The order of the breath-hold multi-slice 2D and the 3D acquisitions were randomized, with a 40 to 50 minute wait between the two perfusion scans.

**Image Reconstruction—**The k-space data were exported and transferred to a stand-alone workstation for further analysis. The proposed reconstruction was performed off-line as described above. Comparison images were generated via three different $B_1$-weighted reconstructions using the same coil sensitivity maps: a) Zero-filling of the measured data, where the k-space lines that were not acquired were replaced with zero, and an inverse Fourier transform was applied for the zerofilled images, b) Each dynamic was reconstructed individually using TV regularization, referred to as dynamic-by-dynamic reconstruction, c) Deriving a principal component basis for the whole volume from the central k-space lines as in conventional PCA-based techniques (9,24), and using this *x-pc* sparsity for regularization. Flowchart for a single iteration of the $B_1$ weighted algorithms, as well as a summary of the thresholding techniques is depicted in Figure 2. For the $B_1$-weighted reconstructions of the 3D datasets, the data from the edge coils, where folding artifacts may occur due to the limited FOV in the foot-head phase encoding direction, were not included in the $B_1$-weighting. The typical reconstruction times for the MATLAB-only implementation of these techniques were: ~ 20 minutes for the dynamic-by-dynamic TV reconstruction, ~ 45 minutes for the x-pc regularized CS reconstruction, and ~ 90 minutes for the proposed reconstruction (110 minutes including the first TV reconstruction).

## Image and Statistical Analysis

A qualitative assessment of image quality was performed for all 3D reconstructions. All reconstructions were written into DICOM format and imported into ViewForum (Philips Healthcare, Best, NL, vR4.2V1L2) for qualitative evaluation by two experienced blinded reviewers independently, using a four-point scale system: 1, poor or uninterpretable (myocardium, RV and LV boundaries not visible or with markedly blurred borders and

edges); 2, fair (myocardium, RV and LV visible, with moderately blurred borders and edges); 3, good (myocardium, RV and LV visible, with mildly blurred borders and edges); 4, excellent (myocardium, RV and LV visible, with sharply defined borders and edges). Imaging scores are presented as mean ± one standard deviation. The signed rank test was used for imaging scores in pair-wise fashion to test for the null hypothesis that the central tendency of the difference was zero for the proposed and other reconstructions. All statistical analyses were performed using SAS (v9.3, SAS Institute, Cary, NC). A $P$ value of $<0.05$ was considered to be significant.

For the four healthy volunteers, for which both an accelerated 3D acquisition and a breath-hold multi-slice 2D perfusion with parallel imaging were acquired, region-based time intensity curve analyses was performed. The analysis was performed on the mid-short-axis slice of the 3D volume and the 2D stack (21), using QMASS MR (v7.2, Medis, Leiden, The Netherlands). The endocardial and epicardial contours were drawn on each dynamic several pixels from the outer and inner borders to limit signal contamination. The contrast uptake curves were then generated for the LV blood pool and the myocardium for the commercially available SENSE reconstruction for the multi-slice 2D acquisition and the proposed reconstruction for the 3D acquisition.

## Results

Rest first-pass perfusion CMR was successfully completed in all subjects without complications. Figure 3 depicts the results of the pilot study in a 3D dataset to determine the first-stage estimate which would be used to generate the distinct pc bases for the proposed regularization, comparing a dynamic-by-dynamic spatial TV reconstruction to a low-resolution image generated from the central k-space. The starting images based on the two techniques are shown in Figure 3a, where significant partial voluming effects are observed for the low-resolution image. The corresponding reconstructions using the proposed regularization based on the pc bases derived from these images are depicted in Figure 3b. Improvement in reconstruction quality is visualized when the pc bases are derived from the spatial TV regularized reconstruction, which is used for the first stage of the algorithm in all subsequent reconstructions.

Figure 4 shows various reconstructions of all the slices of the multi-slice 2D acquisition in an example dynamic after the contrast arrival in the LV. Reconstructions using the dynamic-by-dynamic TV reconstruction ($2^{nd}$ row) removes a substantial amount of the ghosting artifacts along the phase encode direction apparent in the acquired data ($1^{st}$ row), however it is still blurry due to the high undersampling rate. The x-pc reconstruction ($3^{rd}$ row) and the proposed reconstruction ($4^{th}$ row) both yield sharper images. The proposed reconstruction shows more signal homogeneity in the LV and RV blood pools compared to the x-pc reconstruction, potentially due to a reduction in the reconstruction artifacts based on the regularization, in view of the free-breathing nature of the acquisition.

Figure 5 shows example slices of a highly-undersampled 3D acquisition from a patient in a dynamic after contrast arrival. The dataset was acquired with breath-holding at the time of injection, hence it includes both free-breathing and breath-hold dynamics. The dynamic-by-

dynamic TV reconstruction has limited use in removing the aliasing, and incurs spatial blurring artifacts due to the high undersampling rate. The x-pc regularized reconstruction is sharper compared to the TV reconstruction, but there are residual artifacts due to the free-breathing dynamics. The proposed reconstruction shows good temporal fidelity with clearly defined blood-myocardium borders. Figure 6 shows example slices of a 3D dataset from another subject. This dataset was also acquired with a mix of free-breathing and breath-hold dynamics, with breath-holding at the time of injection. The TV reconstruction removes some of the aliasing artifacts from the acquired image. Sharper images are obtained with the x-pc regularized reconstruction, although residual artifacts are apparent. The proposed reconstruction leads to a sharp and less noisy image compared to the other reconstructions.

Figure 7 shows examples dynamics of the middle slices of the 3D volume from a subject, where the acquisition was free-breathing throughout the scan. Due to the high undersampling rate, the dynamic-by-dynamic TV reconstruction suffers from spatial blurring, even though some of the aliasing artifacts have been suppressed compared to the zerofilled acquisition data. The x-pc reconstruction suffers from residual respiratory motion due to temporal blurring. The proposed method offers a clearer visualization of the LV and RV, as well as the myocardium even in the presence of respiratory motion. Overall qualitative image scores demonstrate that the proposed method (2.8±0.5) is significantly better than x-pc regularized CS (2.3±0.5, $P < 0.01$), dynamic-by-dynamic TV-regularized CS (1.7±0.5, $P < 0.01$), and the zerofilled images (1.1±0.2, $P < 0.01$).

Figure 8 depicts example images corresponding to the peak RV, LV and myocardial enhancement across all slices, using the 7.5-fold accelerated 3D acquisition with the proposed reconstruction (a), and 2.7-fold accelerated multi-slice breath-hold 2D acquisition using the commercially available SENSE reconstruction (b) in a healthy subject. The corresponding signal intensity curves indicate similar dynamics of contrast uptake both in the LV blood pool (c) and across the myocardium (d).

## Discussion

In this study, we proposed and evaluated a CS-based reconstruction technique for CMR perfusion that utilizes local information in both spatial and temporal domains, and that can be applied to highly-accelerated free-breathing multi-slice 2D and 3D myocardial perfusion. The proposed reconstruction uses coil sensitivity information and sparsity regularization based on an overcomplete representation obtained by deriving distinct principal component bases for each $N_b \times N_b \times 1 \times N_{dyn}$ overlapping image volume in the $B_1$-weighted image.

The feasibility of the proposed reconstruction method was first evaluated in multi-slice 2D perfusion, and its efficacy was subsequently implemented in 3D perfusion. The nature of these acquisitions is vastly different. In multi-slice 2D, a 4-fold acceleration is sufficient to acquire each slice with sufficient temporal window of ~150 ms for the given imaging parameters. For 3D imaging, however, a substantially higher acceleration rate of 7.5-fold is necessary to acquire the volume in a temporal window of 250 ms. Even in the presence of higher SNR for 3D acquisitions, this higher rate may hinder the reconstruction progress. The effects of the higher acceleration rate were apparent in the reconstructions presented. While

in multi-slice 2D, the difference between x-pc and the proposed reconstruction was most apparent in signal homogeneity, in 3D acquisitions, the difference was larger, where the proposed method provided shaper borders, which at times were not visualized with the other reconstructions.

Previous applications of CS to randomly undersampled 3D perfusion imaging have been limited to regularization using *x-f* sparsity or spatio-temporal TV norm (22,28). For 2D datasets acquired with a combination of breath-holds and free-breathing, these regularization techniques tend to suffer from respiratory artifacts (12). In this work, by using a technique that uses localized spatio-temporal acquisition, the feasibility of randomly undersampled 3D perfusion with free-breathing acquisitions was established.

The proposed technique uses a two-step procedure of first generating a basic estimate and then utilizing this estimate for generating the principal component bases for each localized spatio-temporal volume. The two-step procedure has been previously utilized in dynamic MRI, where the initial estimate has been generated using *x-f* space sparsity (14,24,29). In this work, we chose to use TV norm regularization for each dynamic individually in order to avoid possible temporal blurring artifacts due to the use of a spatio-temporal regularizer. The dynamic-by-dynamic TV reconstruction sufficiently suppresses ghosting artifacts related to random undersampling at the cost of spatial blurring for the acceleration rates used in this study. However, if higher acceleration rates are utilized, a dynamic-by-dynamic TV reconstruction may not sufficiently suppress the aliasing artifacts. An alternative is to use low-resolution image generated from the central k-space as in (20). However, our results indicate that for the small center size used in this study for 3D datasets, these low-resolution images suffer from partial voluming artifacts and hence do not have sufficient spatial resolution to generate principal component bases of adequate qualify for effective utilization of the spatio-temporal localization. Further studies are needed to determine the utility of low-resolution images with larger central k-space sampling in determining the principal component bases for higher acceleration rates.

An alternative technique for the two-step procedure is the use of low-rank constraints for reconstruction of dynamic MRI (12,30). These techniques vectorize each time frame and arrange these time frames into a matrix, which may have low-rank properties. The rank of such a matrix is upper-bounded by the number of dynamics used in the formation of the matrix. The low-rank assumption further assumes that there exists a matrix that closely approximates this matrix with a much smaller rank. In our case, we use matrices of size $100 \times 5$, as determined by the choice of block size for the 2D patches and the temporal extent to which correlations are exploited. These matrices inherently have a rank of at most 5, even in the presence of aliasing artifacts. Due to this low rank, the low-rank techniques were found to be not applicable to this problem in a preliminary study (data not shown). However, the rank regularization techniques have the advantage of not relying on previous estimates, as well as the use of singular vectors in both spatial and temporal directions. Hence, the use of rank regularization techniques for smaller block-sizes or larger temporal windows warrant further investigation.

A possible extension to the proposed algorithm is to use different patch sizes according to the image content. For relatively uniform areas such as the blood pools, a larger patch size can be utilized, whereas for myocardium, one can use smaller patches. Use of shape-adaptive patches may further improve the adaptability of the algorithm (31). These approaches might be useful in reducing the reconstruction time or increasing the reconstruction quality by incorporating further prior information. However, this was not studied in the current study.

In our study, the size of the fully-acquired central k-space was not systematically studied, which is especially important in accelerated 3D perfusion. In our previous experience with CS in segmented 3D acquisitions, we have developed an empirical rule-of-thumb of sampling the central k-space corresponding to ~ 4–5 % of the whole k-space. However, with an undersampling rate of 7.5 for the 3D acquisitions and an elliptical shutter, this would require approximately half of the acquired lines to be sampled from the center of k-space. Hence, based on our initial reconstructions, we have opted to acquire 30% of our data from the central k-space, which may be insufficient. Alternatively, an elliptical shutter might be applied to the central lines as well instead of acquiring a fully-sampled rectangle. However, this approach was not implemented for this study.

For the CS reconstructions in this study, the weights of the regularization terms and thus the corresponding thresholding parameters were chosen empirically as in other CS studies (11,23,24,29). Furthermore, for the proposed algorithm, there are additional parameters, $N_b$ and $N_{dyn}$ that needs to be chosen a-priori. The effects of varying this parameter were studied by varying $N_b$ among {5, 10, 20}, and $N_{dyn}$ among {3, 5, 10}, and performing the proposed reconstruction for each of these 9 pairs of ($N_b$, $N_{dyn}$). Based on this study (results not shown), for small $N_b$ or $N_{dyn}$, it is difficult to remove aliasing artifacts leading to blurrier images. Similarly for large $N_b$ or $N_{dyn}$, the reconstruction introduces spatial or temporal blurring respectively, with the x-pc CS reconstruction representing the limiting case of using the whole volume. Thus, we have empirically set these parameters for an adequate trade-off between removing aliasing artifacts and avoiding spatio-temporal blurring due to signal averaging.

Our study has limitations. More spatial coverage of the LV and improved spatial resolution may be necessary for the identification of perfusion defects or to avoid dark rim artifacts (32). The temporal resolution of the 3D acquisitions may still be longer than the quiescent period of the heart, and thus these acquisitions may be susceptible to cardiac motion. We have not provided comparisons against the currently used compartment-based k-t PCA reconstruction. This reconstruction is designed to work with uniform undersampling, which conflicts with the random undersampling used in this study, and hence requires an extra acquisition. We have not provided SNR/CNR measurements since CS algorithms inherently threshold the noise, making it difficult to locally characterize the noise in the reconstructions. Further clinical studies are needed to assess its diagnostic value in patients with suspected coronary artery disease, as well as in subjects with highly irregular breathing patterns or in the presence of exercise stress.

## Conclusion

We have demonstrated a reconstruction technique that utilizes coil sensitivity information and sparsity regularization based on localized information in both spatial and temporal domains for highly-accelerated CMR perfusion with potential utility in free-breathing 3D acquisitions.

## Acknowledgments

The project described was supported in part by NIH R01EB008743-01A2, NIH K99HL111410-01.

The authors would like to thank Warren J. Manning, MD for his editorial comments.

## References

1. Atkinson DJ, Burstein D, Edelman RR. First-pass cardiac perfusion: evaluation with ultrafast MR imaging. Radiology. 1990; 174(3 Pt 1):757–762. [PubMed: 2305058]
2. Al-Saadi N, Nagel E, Gross M, Bornstedt A, Schnackenburg B, Klein C, Klimek W, Oswald H, Fleck E. Noninvasive detection of myocardial ischemia from perfusion reserve based on cardiovascular magnetic resonance. Circulation. 2000; 101(12):1379–1383. [PubMed: 10736280]
3. Nagel E, Klein C, Paetsch I, Hettwer S, Schnackenburg B, Wegscheider K, Fleck E. Magnetic resonance perfusion measurements for the noninvasive detection of coronary artery disease. Circulation. 2003; 108(4):432–437. [PubMed: 12860910]
4. Kellman P, Arai AE. Imaging sequences for first pass perfusion --a review. J Cardiovasc Magn Reson. 2007; 9(3):525–537. [PubMed: 17365232]
5. Pruessmann KP, Weiger M, Scheidegger MB, Boesiger P. SENSE: sensitivity encoding for fast MRI. Magn Reson Med. 1999; 42(5):952–962. [PubMed: 10542355]
6. Kellman P, Derbyshire JA, Agyeman KO, McVeigh ER, Arai AE. Extended coverage first-pass perfusion imaging using slice-interleaved TSENSE. Magn Reson Med. 2004; 51(1):200–204. [PubMed: 14705062]
7. Plein S, Radjenovic A, Ridgway JP, Barmby D, Greenwood JP, Ball SG, Sivananthan MU. Coronary artery disease: myocardial perfusion MR imaging with sensitivity encoding versus conventional angiography. Radiology. 2005; 235(2):423–430. [PubMed: 15858084]
8. Tsao J, Boesiger P, Pruessmann KP. k-t BLAST and k-t SENSE: dynamic MRI with high frame rate exploiting spatiotemporal correlations. Magn Reson Med. 2003; 50(5):1031–1042. [PubMed: 14587014]
9. Pedersen H, Kozerke S, Ringgaard S, Nehrke K, Kim WY. k-t PCA: temporally constrained k-t BLAST reconstruction using principal component analysis. Magn Reson Med. 2009; 62(3):706–716. [PubMed: 19585603]
10. Plein S, Kozerke S, Suerder D, Luescher TF, Greenwood JP, Boesiger P, Schwitter J. High spatial resolution myocardial perfusion cardiac magnetic resonance for the detection of coronary artery disease. Eur Heart J. 2008; 29(17):2148–2155. [PubMed: 18641047]
11. Otazo R, Kim D, Axel L, Sodickson DK. Combination of compressed sensing and parallel imaging for highly accelerated first-pass cardiac perfusion MRI. Magn Reson Med. 2010; 64(3):767–776. [PubMed: 20535813]
12. Lingala SG, Hu Y, DiBella E, Jacob M. Accelerated dynamic MRI exploiting sparsity and low-rank structure: k-t SLR. IEEE Trans Med Imaging. 2011; 30(5):1042–1054. [PubMed: 21292593]
13. Prieto C, Usman M, Wild JM, Kozerke S, Batchelor PG, Schaeffter T. Group sparse reconstruction using intensity-based clustering. Magn Reson Med. 2013; 69(4):1169–1179. [PubMed: 22648740]
14. Otazo, R.; Kim, D.; Axel, L.; Sodickson, D. Combination of compressed sensing and parallel imaging with respiratory motion correction for highly-accelerated first-pass cardiac perfusion MRI. 2011 May; Montreal. Proceedings of the 19th Scientific Meeting of ISMRM; p. 66

15. Shaw LJ, Berman DS, Maron DJ, Mancini GB, Hayes SW, Hartigan PM, Weintraub WS, O'Rourke RA, Dada M, Spertus JA, Chaitman BR, Friedman J, Slomka P, Heller GV, Germano G, Gosselin G, Berger P, Kostuk WJ, Schwartz RG, Knudtson M, Veledar E, Bates ER, McCallister B, Teo KK, Boden WE. Optimal medical therapy with or without percutaneous coronary intervention to reduce ischemic burden: results from the Clinical Outcomes Utilizing Revascularization and Aggressive Drug Evaluation (COURAGE) trial nuclear substudy. Circulation. 2008; 117(10):1283–1291. [PubMed: 18268144]
16. Kellman, P.; Zhang, Q.; Larson, A.; Simonetti, O.; McVeigh, E.; Arai, AE. Cardiac first-pass perfusion MRI using 3D trueFISP parallel imaging using TSENSE. 2004 May; Kyoto. Proceedings of the 12th Scientific Meeting of ISMRM; p. 310
17. Shin T, Hu HH, Pohost GM, Nayak KS. Three dimensional first-pass myocardial perfusion imaging at 3T: feasibility study. J Cardiovasc Magn Reson. 2008; 10:57. [PubMed: 19077220]
18. Kellman P, Epstein FH, McVeigh ER. Adaptive sensitivity encoding incorporating temporal filtering (TSENSE). Magn Reson Med. 2001; 45(5):846–852. [PubMed: 11323811]
19. Weiger M, Pruessmann KP, Boesiger P. 2D SENSE for faster 3D MRI. MAGMA. 2002; 14(1):10–19. [PubMed: 11796248]
20. Vitanis V, Manka R, Giese D, Pedersen H, Plein S, Boesiger P, Kozerke S. High resolution three-dimensional cardiac perfusion imaging using compartment-based k-t principal component analysis. Magn Reson Med. 2011; 65(2):575–587. [PubMed: 20928876]
21. Shin T, Nayak KS, Santos JM, Nishimura DG, Hu BS, McConnell MV. Three-dimensional first-pass myocardial perfusion MRI using a stack-of-spirals acquisition. Magn Reson Med. 2013; 69(3):839–844. [PubMed: 22556062]
22. Otazo, R.; Xu, J.; Axel, L.; Sodickson, D. Combination of compressed sensing and parallel imaging for highly-accelerated 3D first-pass cardiac perfusion MRI. 2010 May; Stockholm. Proceedings of the 18th Scientific Meeting of ISMRM; p. 344
23. Akcakaya M, Basha TA, Goddu B, Goepfert LA, Kissinger KV, Tarokh V, Manning WJ, Nezafat R. Low-dimensional-structure self-learning and thresholding: Regularization beyond compressed sensing for MRI Reconstruction. Magn Reson Med. 2011; 66(3):756–767. [PubMed: 21465542]
24. Kim D, Dyvorne HA, Otazo R, Feng L, Sodickson DK, Lee VS. Accelerated phase-contrast cine MRI using k-t SPARSE-SENSE. Magn Reson Med. 2012; 67(4):1054–1064. [PubMed: 22083998]
25. Akcakaya M, Basha TA, Chan RH, Manning WJ, Nezafat R. Accelerated isotropic sub-millimeter whole-heart coronary MRI: Compressed sensing versus parallel imaging. Magn Reson Med. 2013 Epub ahead of print. 10.1002/mrm.24683
26. Figueiredo M, Nowak R. An EM algorithm for wavelet-based image restoration. IEEE Transactions on Image Processing. 2003; 12:906–916. [PubMed: 18237964]
27. Akcakaya M, Basha TA, Chan RH, Rayatzadeh H, Kissinger KV, Goddu B, Goepfert LA, Manning WJ, Nezafat R. Accelerated contrast-enhanced whole-heart coronary MRI using low-dimensional-structure self-learning and thresholding. Magn Reson Med. 2012; 67(5):1434–1443. [PubMed: 22392654]
28. Chen L, Adluru G, Schabel MC, McGann CJ, Dibella EV. Myocardial perfusion MRI with an undersampled 3D stack-of-stars sequence. Med Phys. 2012; 39(8):5204–5211. [PubMed: 22894445]
29. Feng L, Otazo R, Jung H, Jensen JH, Ye JC, Sodickson DK, Kim D. Accelerated cardiac T2 mapping using breath-hold multiecho fast spin-echo pulse sequence with k-t FOCUSS. Magn Reson Med. 2011; 65(6):1661–1669. [PubMed: 21360737]
30. Haldar, JP.; Liang, ZP. Low-rank approximations for dynamic imaging. 2011 April; Chicago, IL. IEEE International Symposium on Biomedical Imaging; p. 1052-1055.
31. Foi A, Katkovnik V, Egiazarian K. Pointwise shape-adaptive DCT for high-quality denoising and deblocking of grayscale and color images. IEEE Transactions on Image Processing. 2007; 16(5): 1395–1411. [PubMed: 17491468]
32. Di Bella EV, Parker DL, Sinusas AJ. On the dark rim artifact in dynamic contrast-enhanced MRI myocardial perfusion studies. Magn Reson Med. 2005; 54(5):1295–1299. [PubMed: 16200553]

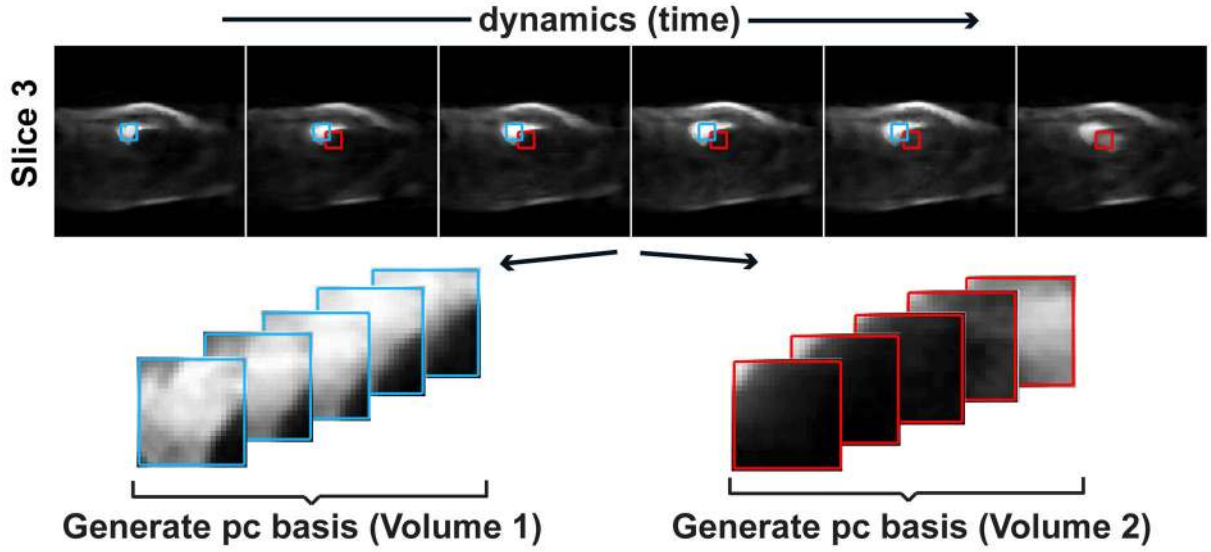


**Figure 1.**

The process of generating the distinct temporal principal component basis for each 10×10×1×5 volume (in *x*-*y*-*z*-*t* space): An initial dynamic-by-dynamic total variation (TV)-regularized estimate is used to localize each such overlapping volume (e.g. the ones containing the blue or red patches). The patches are combined together into a 100×5 matrix, and the right singular vectors are used as the temporal principal component basis for that volume in the proposed reconstruction (pc = principal component).

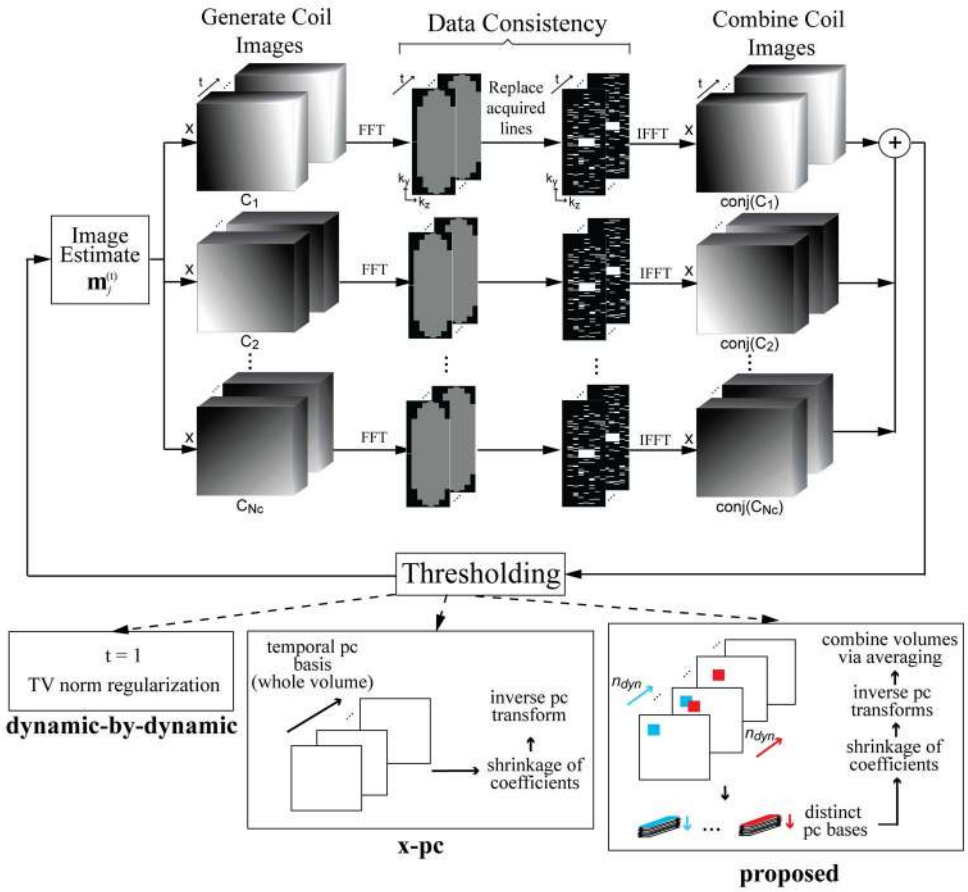


**Figure 2.**

Flowchart for a single iteration of the $B_1$ weighted algorithms used in this study. At every iteration, the current image estimate is mapped to individual coil images by voxel-wise multiplication with sensitivity maps. Data consistency is enforced by replacing the acquired k-space lines study (3D k-space is depicted in the figure). A combined image is generated by summing the voxel-wise product of data-consistent coil images and conjugate of coil sensitivity maps across the coil dimension. This image is then thresholded using one of the three techniques described: dynamic-by-dynamic, x-pc or the proposed regularization.

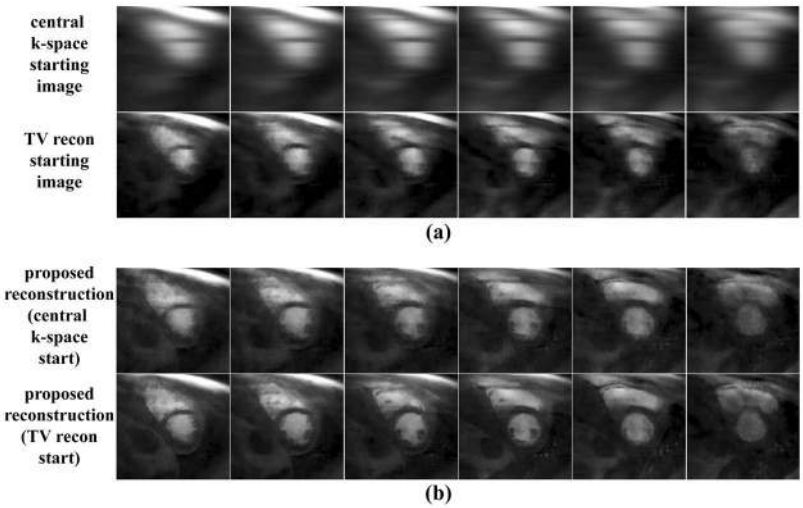


**Figure 3.**

Comparison of using a low-resolution image from the fully-sampled central k-space versus a spatial TV regularized reconstruction to generate the distinct pc bases for the proposed reconstruction in a 3D dataset: (a) The low-resolution images show significant partial voluming effects due to small center size ($11 \times 3$ in $k_y$-$k_z$) compared to the TV reconstruction, (b) The corresponding reconstructions using the proposed regularization indicate visual improvement when the TV reconstruction is used to generate distinct pc bases for each 10×10×1×5 volume.

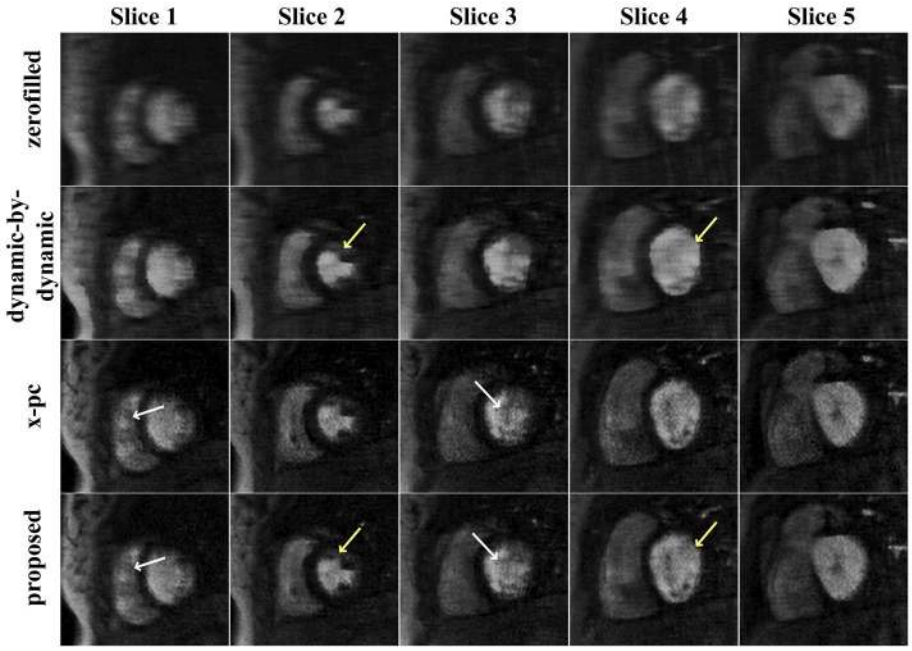


**Figure 4.**

All the slices of the multi-slice 2D acquisition from a healthy subject in a dynamic after the contrast arrival in the left ventricle (LV) during free-breathing. The acquired (zerofilled) data is shown in the top row, suffering from blurriness and aliasing artifacts due to the rate-4 undersampling. Reconstructions using the dynamic-by-dynamic TV reconstruction ($2^{nd}$ row) removes a substantial amount of the ghosting artifacts, however is still blurry due to the high undersampling rate (yellow arrows). The x-pc reconstruction ($3^{rd}$ row) and the proposed reconstruction ($4^{th}$ row) both have sharper edges. The proposed reconstruction shows more signal homogeneity in the LV and RV blood pools compared to the x-pc reconstruction (white arrows).

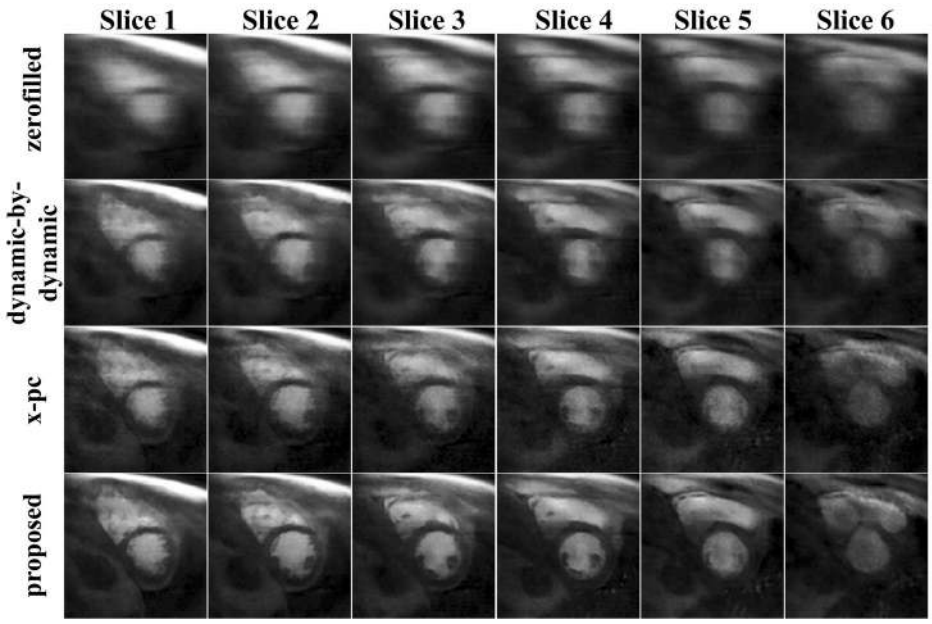


**Figure 5.**

Example slices of a 3D dataset from a subject in a dynamic after the contrast arrival. The acquired (zerofilled) data is shown in the top row. Reconstructions using the proposed method (last row) have good temporal fidelity and are sharper compared to dynamic-by-dynamic compressed sensing (CS) reconstruction (2nd row), and x-pc CS reconstruction (3rd row), which suffer from blurring artifacts.

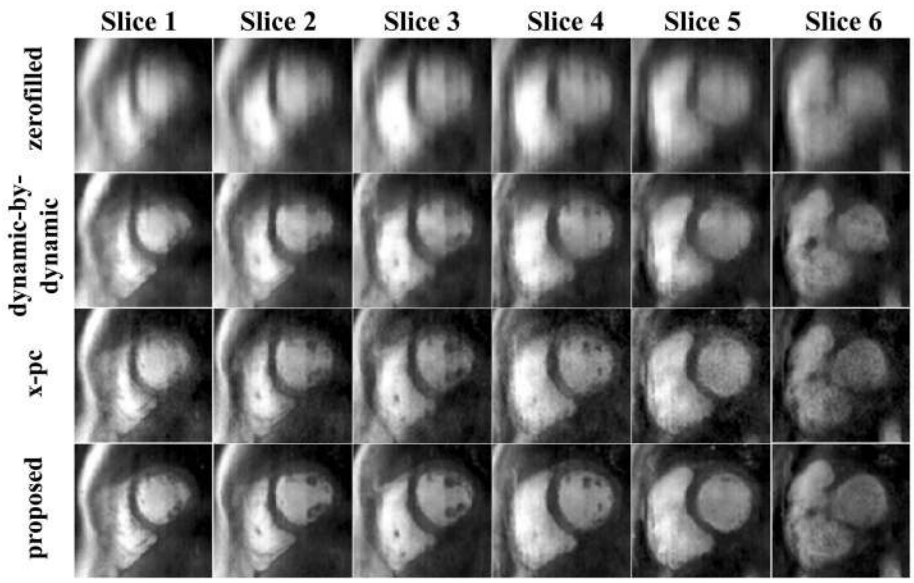


**Figure 6.**

Example slices of a 3D dataset from a subject in a dynamic after the contrast arrival. The blood-myocardium border is more clearly visualized using the proposed method (last row), whereas residual aliasing artifacts are present in the other reconstructions.

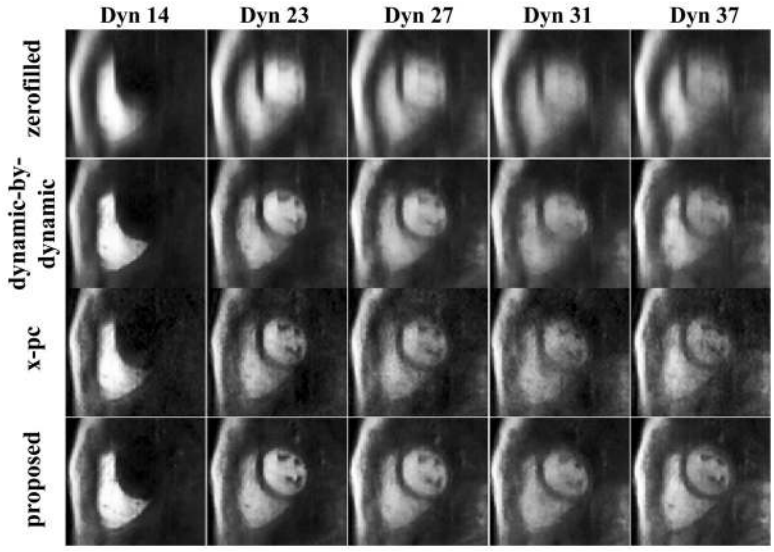


**Figure 7.**

Example dynamics of a middle-section slice from a 3D dataset acquired in free-breathing. The left and right ventricles, as well as the myocardium are delineated using the proposed method even in the presence of respiratory motion (last row). The x-pc reconstruction suffers from residual respiratory motion due to temporal blurring (third row). The dynamic-by-dynamic reconstruction suffers from spatial blurring due to the high undersampling rate (second row).

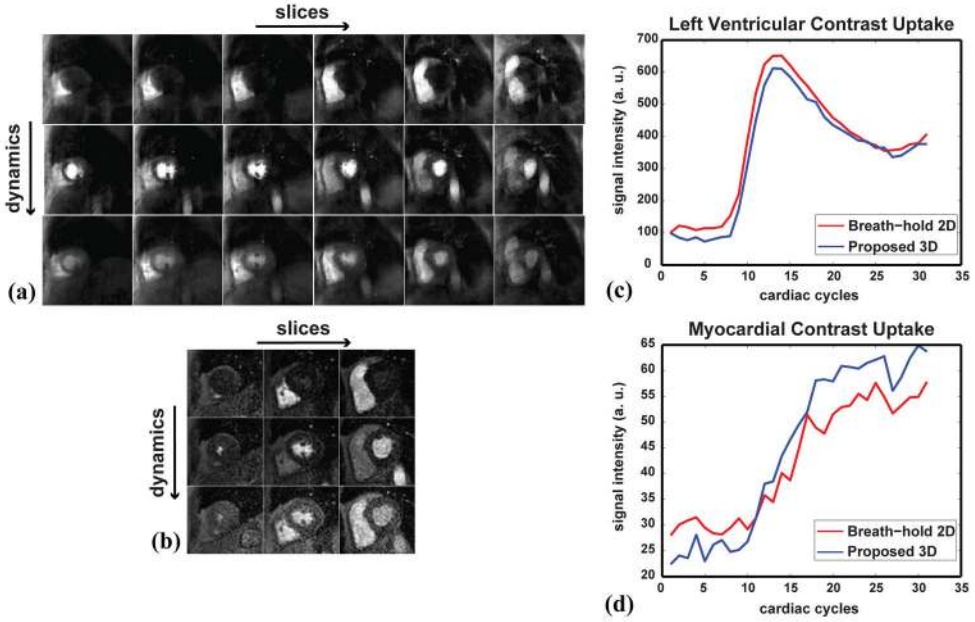


**Figure 8.**

Example images using the 7.5-fold accelerated 3D acquisition with the proposed reconstruction (a), and 2.7-fold accelerated multi-slice breath-hold 2D acquisition using the commercially available SENSE reconstruction (b) in a healthy subject, depicting the peak RV, LV and myocardial enhancement across all slices. The signal intensity curves show similar dynamics of contrast uptake, in the LV blood pool (c) and the myocardium (d). There are differences due to the order of imaging (3D acquisition was performed first during the same examination), as well as due to contrast differences between the reconstruction using the commercially available software, and the raw data reconstruction.